IEEE Control Systems Letters paper presented at
2023 62nd IEEE Conference on Decision and Control (CDC)
December 13-15, 2023. Marina Bay Sands, Singapore

A Novel Finite Difference-based Model Reduction and a Sensor Design for a Multilayer Smart Beam with Arbitrary Number of Layers

Ahmet Kaan Aydın *Member, IEEE*, Ahmet Özkan Özer *Member, IEEE*, and Jacob Walterman,

***Abstract*— A Mead-Marcus type model describing the vibrations on a multilayer smart beam with arbitrary number of layers is considered with hinged boundary conditions. The model is known to be exactly observable in an appropriate Hilbert space with a single boundary sensor measurement. As a standard Finite Differences-based model reduction is considered, it is proved that the model reduction lacks exact observability uniformly as the mesh parameter goes to zero. This is a known phenomenon caused by spurious (artificial) high-frequency eigenvalues. First, it is proved that the exact observability can be retained by the implementation of the direct Fourier filtering technique. However, the optimality of the applied filtering demands further investigation. For this reason, an alternate model reduction is investigated by cleverly reducing the order of the model together with the consideration of equidistant grid points and averaging operators, as in Liu and Guo (2019, 2020, and 2021). This new model reduction successfully retains the exact observability uniformly as as the mesh parameter goes to zero. Moreover, it does not need a further numerical filtering. Our results are based on carefully analyzing the spectrum of the system matrix, and they are applicable to the standard Euler-Bernoulli and Rayleigh beam equations. The numerical simulations are provided to compare reduced models and to show the strength of introduced results.**

***Index Terms*— Computational methods, Order-reduction, Multi-layer beams, Numerical algorithms, Smart structures.**

I. Introduction

For $m \in \mathbb{N}$, consider a multi-layer beam consisting of perfectly bonded alternating $m+1$ stiff layers (piezoelectric/elastic) and m viscoelastic "core" layers. Let the scalar function $z(x,t)$ and the $m \times 1$ column vector $\vec{\mathbf{v}}$ denote the uniform transverse (bending) displacement of the centerlines of layers and the transverse shear angles of viscoelastic layers. Throughout the paper, let dots and primes denote the time derivative $\frac{\partial}{\partial t}$ and $\frac{\partial}{\partial x}$. The equations of motion for the abstract Mead-Marcus-type smart beam [12] hinged at both ends are

$$\begin{cases} \ddot{z} + z'''' - \mathbf{B}^T \vec{\mathbf{v}}' = 0, \\ -\mathbf{C}\vec{\mathbf{v}}'' + \mathbf{P}\vec{\mathbf{v}} = -\mathbf{B}z''', & (x,t) \in (0,L) \times \mathbb{R}^+ \\ z,\ \vec{\mathbf{v}}',\ z''|_{x=0,L} = 0, & t \in \mathbb{R}^+ \\ (z,\dot{z})(x,0) = (z_0,z_1)(x), & x \in (0,L) \end{cases} \tag{1}$$

where the $\mathbf{B} \in \mathbb{R}^m$ is a column vector with positive entries, $\mathbf{C}, \mathbf{P} \in \mathbb{R}^{m \times m}$ are invertible, symmetric, positive definite matrices. All three matrices are defined in terms of shear moduli, Young's moduli, Poisson's ratios, mass densities, and thicknesses of the layers, e.g. see [1], [3], [12] and the references therein about the modeling assumptions of (1).

The exact boundary observability of the abstract PDE model (1) with clamped boundary conditions in an appropriate Hilbert space is studied by the multipliers approach for the first time [12]. For hinged boundary conditions, the exact controllability is first studied in [13] where the boundary observation (sensor measurement) is not provided explicitly due to the nature of the moment method being used in the proofs. The exact observability result for (1) with the explicit description of the boundary observation is recently proved for arbitrary number of layers in [11]. In fact, the explicit description of the boundary observation is deeply needed in practical engineering applications to design the boundary sensor in its finite-dimensional model reduction.

The literature on finding robust finite-dimensional model reductions for PDE models suggests that the available computational techniques are not mathematically rigorous or reliable if one "blindly" implements highly popular approximation methods, e.g. Finite Differences or Finite Elements. Indeed, implementing these approximations result in spurious unobservable (high-frequency) vibrational modes in the approximated dynamics; see [15] for a detailed discussion. Therefore, the finite dimensional model reductions do not retain exact observability uniformly as the discretization parameter approaches zero. These unobservable high-frequency modes can be eliminated by either of the *"direct Fourier filtering"* or *"indirect filtering"* methods [4]. Direct Fourier filtering is shown to be more efficient than the indirect filtering since it encompasses both low and high-frequency eigenvalues, while ignoring spurious eigenvalues. In fact, direct Fourier filtering is successfully applied to the single Euler-Bernoulli [5] and Rayleigh [10] beam models with hinged boundary conditions. A Finite Differences-based model reduction of (1) with only

The work of A.Ö. Özer was supported by the National Science Foundation under Cooperative Agreement No. 1849213.

Ahmet Kaan Aydın is currently with Department of Mathematics, University of Maryland, Baltimore County, Baltimore, MD 21250, USA (e-mail: aaydin1@umbc.edu).

Ahmet Özkan Özer and Jacob Walterman are with Department of Mathematics, Western Kentucky University, Bowling Green, KY 42101, USA. (e-mail: ozkan.ozer@wku.edu), (e-mail: jacob.walterman061@topper.wku.edu).

three-layers, i.e. $\mathbf{B}, \mathbf{C}, \mathbf{P} \in \mathbb{R}^+$ in (1), is proposed for the first time in [11]. Utilizing the direct Fourier filtering technique, the uniform observability result is proved in the lower-order energy space.

Even though the direct Fourier filtering method works well with known PDE models, the major drawback is that the whole spectrum of eigenvalues must be known explicitly. Moreover, the optimality of the applied filtering must be addressed. Recently, a novel Finite Differences-based model reduction is proposed for the wave equation and the standard Euler-Bernoulli beam model [6]-[8],[14]. The model is constructed using equidistant grid points and averaging operators, and thus, no filtering is necessary. The uniform observability result is proved by the discrete multipliers method, which seems to be particularly compatible with cantilevered boundary conditions (as the spectrum can not be determined explicitly). However, the major drawback is that the observation time is suboptimal, i.e. $T > T^* = 2$, even though the PDE counterpart is known to be observable for any $T > T^* = 0$.

In this paper, (i) the Finite Differences-based model reductions of (1) in [11] are extended from three layers to multi-layers with arbitrary number of layers. (ii) As the spectrum is determined explicitly in terms of the matrices $\mathbf{B}, \mathbf{C}, \mathbf{P}$, the exact observability result is proved uniformly as the discretization parameter $h \to 0$. (iii) Next, which is the major contribution of this work, the exact observability of the model reduction of (1), constructed using equidistant grid points and averaging operators, is rigorously established without the need of numerical filtering by the spectral approach, discarding the multipliers approach in [6], [7] completely. (iv) More importantly, the observability result for each model reduction is shown to hold true for any $T > T^* = 0$. Finally, to compare the strength of the proposed model reductions, simulations are provided with the design of a stabilizing feedback controller. Our results not only extend the results in [5], [6], [7], [11] from a single-layer beam to multi-layer beams with arbitrary number of layers but also provide better insights to understand the overall observability/sensor design of multi-layer beams.

II. State-Space Formulation and Exact Observability

Note that the second equation in (1) is elliptic, and it can be solved for shear angle $\vec{v}$. Letting the differential operator $D_x^2 = \frac{\partial^2}{\partial x^2}$ be defined on the domain

$$\mathrm{Dom}(D_x^2) = \{z \in H^2(0,l) \mid z_x(0) = z_x(L) = 0\}, \qquad (2)$$

the operator $(-\boldsymbol{C}D_x^2 + \boldsymbol{P}) : \mathrm{Dom}(D_x^2) \to L^2(0,L)$ is boundedly invertible. Therefore, the operator $J = \boldsymbol{B}^T(-\boldsymbol{C}D_x^2 + \boldsymbol{P})^{-1}\boldsymbol{B}$ exists and is bounded. By eliminating $\vec{v}$, (1) can be rewritten as

$$\begin{cases} \ddot{z} + (I+J)z'''' = 0, (x,t) \in (0,L) \times \mathbb{R}^+ \\ z(x,t),\ z''(x,t)|_{x=0,L} = 0,\ t \in \mathbb{R}^+ \\ z(x,0) = z^0(x),\ \dot{z}(x,0) = z^1(x),\ x \in (0,L). \end{cases} \qquad (3)$$

The natural energy of (1) is defined on the Hilbert space $\mathcal{H} = [H^2(0,L) \cap H_0^1(0,L)] \times L^2(0,L)$ as the following

$$E(t) = \frac{1}{2}\int_0^L \left[|\dot{z}|^2 + |z''|^2 + (Jz''')z'\right] dx. \qquad (4)$$

Now, define the Hilbert spaces $H_*^3(0,L) = \{z \in H^3(0,L) \cap H_0^1(0,L) : z''|_{x=0,L} = 0\}$, $\mathcal{H}_1 = H_*^3(0,L) \times H_0^1(0,L)$. Define also the higher-order energy of solutions of (1) on the Hilbert space $\mathcal{H}_1 = H_*^3(0,L) \times H_0^1(0,L)$ by

$$E_1(t) := \frac{1}{2}\int_0^L \left[|\dot{z}'|^2 + |z'''|^2 + (Jz''')z'''\right] dx. \qquad (5)$$

Now, the main exact observability result is as the following.

Theorem 1. *The energy $E_1(t)$ is conservative along trajectories of solutions of (1), i.e. $E_1(t) = E_1(0)$, $\forall t \geq 0$. Moreover, for any $T > 0$, the system (1) is exactly observable. In particular, there exist $C_1(T), C_2(T) > 0$ such that*

$$C_1(T)E_1(0) \leq \int_0^T |\dot{z}'(L,t)|^2 dt \leq C_2(T)E_1(0). \qquad (6)$$

Proof. Firstly, the conservation of the energy is straightforward. Considering the observation $z'(L,t)$, the exact observability result for (1) in the Hilbert space $\mathcal{H}_{-1} = H_0^1(0,L) \times H^{-1}(0,L)$ is already established in [11, Theorem 7]. In particular, for any $T > 0$, the system (1) is exactly observable, i.e. there exist $C_3(T), C_4(T) > 0$ such that

$$C_3(T)E_{-1}(0) \leq \int_0^T |z'(L,t)|^2 dt \leq C_4(T)E_{-1}(0) \qquad (7)$$

where the lower-order energy $E_{-1}(t)$ can be defined by

$$E_{-1}(t) := \tfrac{1}{2}\int_0^L \left[|(\partial_x^{-2}\dot{z})'|^2 + |z'|^2 + (Jz')z'\right] dx, \qquad (8)$$

and ∂_x^{-2} denotes the inverse of the isometric anti-isomorphism $\partial_x^2 : H_0^1(0,L) \to H^{-1}(0,L)$. The proof of (7) is quite technical and it is based on the non-harmonic series approach. On the other hand, this result is a foundation for our proof here since $\mathcal{H}_{-1}$ is the dual space of $\mathcal{H}_1$ pivoted with respect to the Hilbert space $\mathcal{H} = [H^2(0,L) \cap H_0^1(0,L)] \times L^2(0,L)$ with the continuous inclusion $\mathcal{H}_1 \subset \mathcal{H} \subset \mathcal{H}_{-1}$. Therefore, the result (6) holds true for the replacement $(\dot{z}, z) \to (\dot{z}'', z'')$ in (7) with the observation $\|z'''(L,t)\|_{L^2(0,T)}$. Notice that the observations $\|z'''(L,t)\|_{L^2(0,T)}$ and $\|\dot{z}'(L,t)\|_{L^2(0,T)}$ are equivalent to the energy norm in $\mathcal{H}_1$. For the purpose of obtaining numerical algorithms by the Order-Reduction technique, we prefer to go by $\|\dot{z}'(L,t)\|_{L^(0,T)}$. Therefore, (6) proceeds. □

III. Model reductions in the Space Variable x

Let $N \in \mathbb{N}$ be given, and define the mesh size $h := \frac{1}{N+1}$. Consider a uniform discretization of the interval $[0,L]$: $0 = x_0 < x_1 < ... < x_{N-1} < x_N < x_{N+1} = L$ Let $z_j = z_j(t) \approx z(x_j,t)$ the approximation of the solution $z(x,t)$ of (3) at the point space $x_j = jh$ for any $j = 0,1,...,N,N+1$, and $\vec{z} = [z_1, z_2, ..., z_N]^T$. Then, we consider the space discretization of Laplace's equation $z''(x_j) \approx (-A_h\vec{z})_j$ where A_h is a tridiagonal $N \times N$ matrix defined by $A_h := \frac{1}{h^2}\mathrm{tridiag}(-1,2,-1)$, whose eigen-pairs $(\lambda_k(h), \vec{\phi}_k(h))$ are [10]:

$$\begin{cases} \lambda_k(h) = \frac{4}{h^2}\sin^2\left(\frac{k\pi h}{2L}\right), \\ \phi_{k,j} = \sin\left(\frac{jk\pi h}{L}\right), \quad k,j = 1,2,...,N. \end{cases} \qquad (9)$$

A. Standard Finite Differences

Letting $\vec{z} = [z_1, z_2, \ldots, z_N]$, by considering the standard central Finite Differences for the second and fourth-order derivatives, the reduced model for (3) is

$$\begin{cases} \ddot{\vec{z}} + (\boldsymbol{I} + \boldsymbol{J}_h)\boldsymbol{A}_h^2 \vec{z} = 0, \\ z_0 = z_{N+1} = 0,\ z_{-1} = -z_1,\ z_{N+2} = -z_N, \\ (\vec{z}, \dot{\vec{z}})_j(0) = (z_0, z_1)(x_j) \end{cases} \tag{10}$$

where

$$\boldsymbol{J}_h = (\boldsymbol{B}^T \otimes \boldsymbol{I_N})\left(C \otimes \boldsymbol{A}_h + P \otimes \boldsymbol{I}_N\right)^{-1}(\boldsymbol{B} \otimes \boldsymbol{I_N})$$

is a positive definite operator, and $\otimes$ is the Kronecker matrix product. Then, (10) can be reformulated to

$$\frac{d}{dt}\begin{bmatrix}\vec{z}\\ \dot{\vec{z}}\end{bmatrix} = \begin{bmatrix}\boldsymbol{0}_{N\times N} & \boldsymbol{I}_{N\times N}\\ -(\boldsymbol{I}+\boldsymbol{J}_h)\boldsymbol{A}_h^2 & \boldsymbol{0}_{N\times N}\end{bmatrix}\begin{bmatrix}\vec{z}\\ \dot{\vec{z}}\end{bmatrix} := \boldsymbol{\mathcal{A}}_{\text{FD}}\begin{bmatrix}\vec{z}\\ \dot{\vec{z}}\end{bmatrix}.$$

Following lemma shows eigen-pairs of $\boldsymbol{\mathcal{A}}_{\text{FD}}$ which can be used to express the solutions to (10).

Lemma 2. *Letting $K := \{-N, ..., -1, 1, ...N\}$, the eigen-pairs $\{(\tilde{\omega}_k(h), \vec{\varphi}_k(h))\}_K$ of $\boldsymbol{\mathcal{A}}_{FD}$ are*

$$(\tilde{\omega}_k(h), \vec{\varphi}_k(h)) = \left(i\sqrt{\mu_k(h)}, \begin{bmatrix}\frac{1}{i\sqrt{\mu_k(h)}}\vec{\phi}_k(h)\\ \vec{\phi}_k(h)\end{bmatrix}\right)$$

where $\mu_k(h)$ are the eigenvalues of $(\boldsymbol{I} + \boldsymbol{J}_h)\boldsymbol{A}_h^2$ defined as for $k = 1, 2, ..., N$,

$$\mu_k(h) = (1 + \omega_k(h))\,\lambda_k^2(h),$$
$$\omega_k(h) = \frac{(\boldsymbol{B}^T\boldsymbol{B})^2}{\lambda_k(h)\boldsymbol{B}^T\boldsymbol{C}\boldsymbol{B} + \boldsymbol{B}^T\boldsymbol{P}\boldsymbol{B}}$$

with $\sqrt{\mu_k(h)} := -\sqrt{\mu_{-k}(h)}$ and $\vec{\varphi}_k := \vec{\varphi}_{-k}$ for $k = -1, -2, ..., -N$. The solutions to (10) can be expressed as

$$\vec{z}(t) = \sum_{k\in K}(a_k e^{i\sqrt{\mu_k(h)}t})\vec{\phi}_k(h). \tag{11}$$

Proof. First, we claim that $(\boldsymbol{B} \otimes \boldsymbol{I}_N)\,\phi_k$ are eigenvectors of $(\boldsymbol{C} \otimes \boldsymbol{A}_h + \boldsymbol{P} \otimes \boldsymbol{I}_N)$ such that

$$(\boldsymbol{C} \otimes \boldsymbol{A}_h + \boldsymbol{P} \otimes \boldsymbol{I}_N)(\boldsymbol{B} \otimes \boldsymbol{I}_N)\,\phi_k = \tilde{\tilde{\lambda}}_k\,(\boldsymbol{B} \otimes \boldsymbol{I}_N)\,\phi_k,$$

where $\tilde{\tilde{\lambda}}_k$ are the corresponding eigenvalues. Multiplying both sides of the equation above by $\phi_k^T(\boldsymbol{B}^T \otimes \boldsymbol{I_N})$ and applying the mixed-product property of Kronecker products undergoing matrix multiplication yields

$$\begin{aligned}
&\phi_k^T(\boldsymbol{B}^T \otimes \boldsymbol{I_N})(\boldsymbol{C} \otimes \boldsymbol{A}_h + \boldsymbol{P} \otimes \boldsymbol{I}_N)(\boldsymbol{B} \otimes \boldsymbol{I}_N)\,\phi_k \\
&\quad = \tilde{\tilde{\lambda}}_k\phi_k^T(\boldsymbol{B}^T \otimes \boldsymbol{I_N})(\boldsymbol{B} \otimes \boldsymbol{I}_N)\,\phi_k, \\
&\phi_k^T\left(\boldsymbol{B}^T\boldsymbol{C}\boldsymbol{B} \otimes \lambda_k\boldsymbol{I}_N + \boldsymbol{B}^T\boldsymbol{P}\boldsymbol{B} \otimes \boldsymbol{I}_N\right)\phi_k \\
&\quad = \tilde{\tilde{\lambda}}_k\phi_k^T(B^TB \otimes \boldsymbol{I_N})\phi_k, \\
&\phi_k^T\left((\lambda_k\boldsymbol{B}^T\boldsymbol{C}\boldsymbol{B} + \boldsymbol{B}^T\boldsymbol{P}\boldsymbol{B}) \otimes \boldsymbol{I}_N\right)\phi_k = \tilde{\tilde{\lambda}}_k\boldsymbol{B}^T\boldsymbol{B}\phi_k^T\phi_k.
\end{aligned}$$

Hence $\tilde{\tilde{\lambda}}_k = \frac{\lambda_k\boldsymbol{B}^T\boldsymbol{C}\boldsymbol{B} + \boldsymbol{B}^T\boldsymbol{P}\boldsymbol{B}}{\boldsymbol{B}^T\boldsymbol{B}}$ such that $(\tilde{\tilde{\lambda}}_k, (\boldsymbol{B} \otimes \boldsymbol{I}_N)\,\phi_k)$ are eigen-pairs of $(\boldsymbol{C} \otimes \boldsymbol{A}_h + \boldsymbol{P} \otimes \boldsymbol{I}_N)$. This implies $(\frac{1}{\tilde{\tilde{\lambda}}_k}, (\boldsymbol{B} \otimes \boldsymbol{I}_N)\,\phi_k)$ are the eigen-pairs of $(\boldsymbol{C} \otimes \boldsymbol{A}_h + \boldsymbol{P} \otimes \boldsymbol{I}_N)^{-1}$. Therefore,

$$\boldsymbol{J}_h\phi_k = \frac{1}{\tilde{\tilde{\lambda}}_k}(\boldsymbol{B}^T \otimes \boldsymbol{I_N})(\boldsymbol{B} \otimes \boldsymbol{I}_N)\,\phi_k = \frac{\boldsymbol{B}^T\boldsymbol{B}}{\tilde{\tilde{\lambda}}_k}\phi_k$$

implies that (ω_k, ϕ_k) are the eigen-pairs of $\boldsymbol{J}_h$ with

$$\omega_k = \frac{(\boldsymbol{B}^T\boldsymbol{B})^2}{\lambda_k\boldsymbol{B}^T\boldsymbol{C}\boldsymbol{B} + \boldsymbol{B}^T\boldsymbol{P}\boldsymbol{B}}. \tag{12}$$

Observe that $\boldsymbol{J}_h$ and $\boldsymbol{A}_h$ have the same eigenvectors, so they are simultaneously diagonalizable. It is straightforward to calculate the eigenvalues of $(\boldsymbol{I}+\boldsymbol{J}_h)\boldsymbol{A}_h^2$ by the eigenvalues of $\boldsymbol{J}_h$ and $\boldsymbol{A}_h$. □

Since the solutions can be expressed by the eigen-pairs, the energy and the sensor measurements can likewise be expressed in terms of eigen-pairs by substituting with the solution. First consider, the discretization of the higher-order energy (5) is

$$\begin{aligned}
E_{h,1}(t) := &\frac{h}{2}\sum_{j=1}^{N}\left|\frac{\dot{\vec{z}}_{j+1} - \dot{\vec{z}}_j}{h}\right|^2 + \left|\frac{(\boldsymbol{A}_h z)_{j+1} - (\boldsymbol{A}_h z)_j}{h}\right|^2 \\
&+ \left(\frac{(\boldsymbol{J}_h\boldsymbol{A}_h^2\vec{z})_{j+1} - (\boldsymbol{J}_h A_h^2\vec{z})_j}{h}\right)\left(\frac{\vec{z}_{j+1} - \vec{z}_j}{h}\right).
\end{aligned} \tag{13}$$

The following lemma shows the conservation of energy and expression of (13) in terms of eigen-pairs.

Lemma 3. *The energy $E_{h,1}(t)$ is conserved along the trajectories , i.e. $\frac{dE_{h,1}(t)}{dt} = 0$. and thus, $E_{h,1}(t) \equiv E_{h,1}(0), \forall t \geq 0$. Moreover, $E_{h,1}(t)$ can be written in terms of eigenvectors as the following*

$$E_{h,1}(t) = h\sum_{k\in K}\sum_{j=0}|\mu_k(h)||a_k|^2\left|\frac{\phi_{k,j+1} - \phi_{k,j}}{h}\right|^2. \tag{14}$$

Proof. To show conservation of energy consider $\frac{dE_{h,1}(t)}{dt}$ and substitute $\ddot{\vec{z}} = -(\boldsymbol{I} + \boldsymbol{J}_h)\boldsymbol{A}_h^2\vec{z}$ such that

$$\begin{aligned}
\frac{dE_{h,1}(t)}{dt} = &h\sum_{j=1}^{N}\left(\frac{(\boldsymbol{A}_h^2\dot{\vec{z}})_{j+1} - (\boldsymbol{A}_h^2\dot{\vec{z}})_j}{h}\right)\left(\frac{\vec{z}_{j+1} - \vec{z}_j}{h}\right) \\
&+ \left(\frac{((\boldsymbol{I}+\boldsymbol{J}_h)\boldsymbol{A}_h^2\vec{z})_j - ((\boldsymbol{I}+\boldsymbol{J}_h)\boldsymbol{A}_h^2\vec{z})_{j+1}}{h}\right)\left(\frac{\dot{\vec{z}}_{j+1} - \dot{\vec{z}}_j}{h}\right) \\
&+ \left(\frac{(\boldsymbol{J}_h\boldsymbol{A}_h^2\vec{z})_{j+1} - (\boldsymbol{J}_h\boldsymbol{A}_h^2\vec{z})_j}{h}\right)\left(\frac{\dot{\vec{z}}_{j+1} - \dot{\vec{z}}_j}{h}\right) = 0,
\end{aligned}$$

which implies $E_{h,1}(t) \equiv E_{h,1}(0), \forall t \geq 0$. Recall that $\boldsymbol{A}_h$ and $\boldsymbol{J}_h$ are simultaneously diagonalizable, and are thus commutative with respect to matrix multiplication. The eigenvalues of $\boldsymbol{J}_h$, and $\boldsymbol{A}_h$ are $\omega_k(h)$, and $\lambda_k(h)$ respectively, for $k \in K$. By the direct substitution of the solution formula (11) into $E_{h,1}(0)$, a straightforward calculation leads to (14). □

Since $\dot{z}_{N+1} = 0$ in (10), observe that the sensor measurement $\int_0^T |\dot{z}'(L,t)|^2\,dt$ can be expressed in terms of the eigenvectors as follows

$$\int_0^T\left|\frac{\dot{z}_N}{h}\right|^2 dt = T\sum_{k\in K}|\mu_k(h)||a_k|^2\left|\frac{\phi_{k,N}}{h}\right|^2. \tag{15}$$

The following identity is used to show the relation between the sensor measurements and the energy which is needed to prove that (10) lacks uniform observability.

Lemma 4. *[4, Lemma 1.1] For any eigenvector $\vec{\phi}_k(h)$, the following identity holds*

$$h\sum_{j=0}^{N}\left|\frac{\phi_{k,j+1} - \phi_{k,j}}{h}\right|^2 = \frac{2L}{4 - \lambda_k h^2}\left|\frac{\phi_{k,N}}{h}\right|^2. \tag{16}$$

Theorem 5. *For any $T > 0$ the system* (10) *lacks uniform observability as $h \to 0$. In particular,*

$$\lim_{h\to 0} \sup_{\vec{z} \text{ solves (10)}} \frac{E_{h,1}(0)}{\int_0^T \left|\frac{\dot{z}_N}{h}\right|^2 dt} \to \infty. \tag{17}$$

Proof. Consider Lemma 3, (15), (16),

$$E_{h,1}(t) \quad = \sum_{k\in K} \tfrac{2L}{4-h^2\lambda_k(h)} |\mu_k(h)||a_N|^2 \left|\tfrac{\phi_{N,N}}{h}\right|^2.$$

It is sufficient to consider $k = N$ for which $4 - h^2\lambda_k(h) \to 0$ as $h \to 0$. □

The lack of uniform observability for (10) in Theorem 5 is caused by spurious high-frequency eigenvalues i.e. $h^2\lambda_N(h) \to 4$ as $h \to 0$. The direct Fourier filtering method filters these eigenvalues so that solutions in the filtered space retains exact observability uniformly. Given any $\gamma \in (0, 4)$, define the following filtered solution space for $\vec{z}_h$ of (10):

$$\boldsymbol{C}_h(\gamma) := \left\{ \vec{z}_h = \sum_{\lambda_k(h) \le \frac{\gamma}{h^2}} (a_k e^{i\sqrt{\mu_k(h)}t})\vec{\phi}_k(h) \right\}. \tag{18}$$

Theorem 6. *Letting $\gamma \in (0, 4)$, for any $T > 0$, there exist a constant $C = C(T, \gamma) := \frac{2L}{T(4-\gamma)} > 0$ such that*

$$E_{h,1}(0) \le C \int_0^T \left|\frac{\dot{z}_N}{h}\right|^2 dt, \qquad \forall \vec{z} \in \boldsymbol{C}_h(\gamma). \tag{19}$$

Proof. For any given $\gamma \in (0, 4)$, let Λ be the largest eigenvalue $\sqrt{\mu_k(h)}$ such that $\lambda_k(h) \le \gamma h^{-2}$. Therefore there exists $\tilde{k}$ such that $\Lambda = \sqrt{\mu_{\tilde{k}}}$. Letting $\tilde{K} = \{-\tilde{k}, ..., -1, 1, ..., \tilde{k}\}$,

$$\begin{aligned} E_{h,1}(t) &= \sum_{k\in\tilde{K}} \tfrac{2L}{4-h^2\lambda_k(h)} |\mu_k(h)||a_N|^2 \left|\tfrac{\phi_{N,N}}{h}\right|^2 \\ &\le \tfrac{2L}{4-\gamma} \sum_{k\in\tilde{K}} |\mu_k(h)||a_N|^2 \left|\tfrac{\phi_{N,N}}{h}\right|^2 = \tfrac{2L}{T(4-\gamma)} \int_0^T \left|\tfrac{\dot{z}_N}{h}\right|^2 dt. \quad \square \end{aligned}$$

Remark 1. The model (10) can be considered with the following discretization of lower-order energy $E_{-1}(t)$ in (8),

$$\begin{aligned} E_{h,-1}(t) := \tfrac{h}{2} \sum_{j=1}^{N} &\left|\tfrac{(\boldsymbol{A}_h^{-1}\dot{\vec{z}})_{j+1} - (\boldsymbol{A}_h^{-1}\dot{\vec{z}})_j}{h}\right|^2 + \left|\tfrac{z_{j+1}-z_j}{h}\right|^2 \\ &+ \left[\tfrac{(\boldsymbol{J}_h\boldsymbol{A}_h\vec{z})_{j+1} - (\boldsymbol{J}_h\boldsymbol{A}_h\vec{z})_j}{h}\right] \left[\tfrac{(\boldsymbol{A}_h^{-1}\vec{z})_{j+1} - (\boldsymbol{A}_h^{-1}\vec{z})_j}{h}\right), \end{aligned}$$

and the corresponding lower-order sensor measurement $\int_0^T \left|\frac{z_N}{h}\right|^2 dt$, as in [11]. In this setup, Theorems 5 and 6 still hold true by scaling the corresponding energy and sensor measurement by $\frac{1}{\lambda_k}$ due to giving up the regularity of solutions. Thus, the new observability constant in Theorem 6 becomes $C = C(T, \gamma) := \left(1 + \frac{(\boldsymbol{B}^T\boldsymbol{B})^2}{\boldsymbol{B}^T\boldsymbol{P}\boldsymbol{B}}\right) \frac{2L}{T(4-\gamma)} > 0$.

Remark 2. Note that Theorems 5 and 6 extend the analogous results in [11] from three-layer beams to multi-layer beams with arbitrary number of layers. In particular, the eigenvalues of the system matrix $\boldsymbol{\mathcal{A}_{FD}}$ changes significantly due to the strong coupling of bending with the shear angles of each core layer. This is mainly due to $\boldsymbol{B}$, $\boldsymbol{C}$, and $\boldsymbol{P}$ becoming matrices, rather than positive constants.

B. Order-Reduced Finite Differences

In this section we apply a recently introduced approximation technique, the method of Order-Reduced Finite Differences (ORFD) see [6]. Define the following finite averaging and difference operators

$$\begin{aligned} &z_{i+\frac{1}{2}} := \tfrac{z_{i+1}+z_i}{2}, && \delta_x z_{i+\frac{1}{2}} := \tfrac{z_{i+1}-z_i}{h}, \\ &\delta_x^2 z_i := \tfrac{z_{i+1}-2z_i+z_{i-1}}{h^2}, && \delta_x^3 z_{i+\frac{1}{2}} := \tfrac{z_{i+2}-3z_{i+1}+3z_i-z_{i-1}}{h^3}, \\ &\delta_x^4 z_i := \tfrac{z_{i+2}-4z_{i+1}+6z_i-4z_{i-1}+z_{i-2}}{h^4}. \end{aligned}$$

Letting $u(x,t) := \dot{z}(x,t)$, $v(x,t) := z'''(x,t)$, and $y(x,t) = Jz''''(x,t)$ the first equation in (3) can be rewritten as

$$\dot{u} + v' + y = 0 \qquad (0, L) \times (0, \infty). \tag{20}$$

Now, consider the following discretization of (20)

$$\dot{u}_{i+\frac{1}{2}} + \delta_x v_{i+\frac{1}{2}} + y_{i+\frac{1}{2}} = 0. \tag{21}$$

Multiplying (21) with $\frac{h}{2}$ yields

$$\frac{v_{i+1} - v_i}{2} = -\frac{h}{2}\dot{u}_{i+\frac{1}{2}} - \frac{h}{2}y_{i+\frac{1}{2}}. \tag{22}$$

Observe that $\frac{v_{i+1}-v_i}{2} = v_{i+1} - v_{i+\frac{1}{2}} = v_{i+\frac{1}{2}} - v_i$ implies two representations of the left-hand side of (22) in terms of v_{i+1} and v_i. First, substitute $\frac{v_{i+1}-v_i}{2} = v_{i+1} - v_{i+\frac{1}{2}}$ in (22) and shift the indices by one, i.e. $i + 1 \to i$,

$$v_i = v_{i-\frac{1}{2}} - \frac{h}{2}\dot{u}_{i-\frac{1}{2}} - \frac{h}{2}y_{i-\frac{1}{2}}. \tag{23}$$

and next, substitute $\frac{v_{i+1}-v_i}{2} = v_{i+\frac{1}{2}} - v_i$ in (22) to get

$$v_i = v_{i+\frac{1}{2}} + \frac{h}{2}\dot{u}_{i+\frac{1}{2}} + \frac{h}{2}y_{i+\frac{1}{2}}, \tag{24}$$

then subtract (23) from (24) to eliminate v_i

$$v_{i+\frac{1}{2}} - v_{i-\frac{1}{2}} + \tfrac{h}{2}\left(\dot{u}_{i+\frac{1}{2}} + \dot{u}_{i-\frac{1}{2}} + y_{i+\frac{1}{2}} + y_{i-\frac{1}{2}}\right) = 0.$$

Now, multiply this equation by $\frac{1}{h}$, and substitute $u_i = \dot{z}_i$ and $v_{i+\frac{1}{2}} = \delta_x^3 z_{i+\frac{1}{2}}$ to get the equivalent model below

$$\begin{cases} \frac{1}{4}\left(\ddot{z}_{i+1} + 2\ddot{z}_i + \ddot{z}_{i-1}\right) + \delta_x^4 z_i \\ \qquad + \frac{1}{4}\left(y_{i+1} + 2y_i + y_{i-1}\right) = 0, \\ z_0 = 0, \ z_{N+1} = 0 \ z_1 = -z_{-1}, \ z_{N+2} = -z_N, \\ z_j(0) = z^0(x_j), \quad \dot{z}_j(0) = z^1(x_j), \end{cases} \tag{25}$$

where discretization of y is defined as $\vec{y} = \boldsymbol{J}_h\boldsymbol{A}_h^2\vec{z}$. Now, defining a tridiagonal $N \times N$ matrix M by $M := \frac{1}{4}\text{tridiag}(1, 2, 1)$, (25) can be reformulated as

$$\frac{\partial}{\partial t}\begin{bmatrix} z \\ \dot{z} \end{bmatrix} = \begin{bmatrix} 0_{N\times N} & I_{N\times N} \\ -(\boldsymbol{M}^{-1} + \boldsymbol{J}_h)\boldsymbol{A}_h^2 & 0_{N\times N} \end{bmatrix}\begin{bmatrix} z \\ \dot{z} \end{bmatrix} := \boldsymbol{\mathcal{A}}_{\text{OR}}\begin{bmatrix} z \\ \dot{z} \end{bmatrix}.$$

Notice that the eigen-pairs $\{(\tilde{\lambda}_k(h), \vec{\phi}_k(h))\}_K$ of $\boldsymbol{M}$ are $\tilde{\lambda}_k(h) = 1 - \frac{h^2}{4}\lambda_k(h) = 1 - \sin^2\left(\frac{k\pi h}{2L}\right)$, which follows from considering eigen-pairs of $\boldsymbol{A}_h$ with $\boldsymbol{M} = \boldsymbol{I} - \frac{h^2}{4}\boldsymbol{A}_h$.

Lemma 7. *The eigen-pairs $\{(\tilde{\tilde{\omega}}_k, \vec{\tilde{\varphi}}_k)\}_{k\in K}$ of $\boldsymbol{\mathcal{A}}_{OR}$ are*

$$(\tilde{\tilde{\omega}}_k(h), \vec{\tilde{\varphi}}_k(h)) = \left(i\sqrt{\tilde{\mu}_k(h)}, \begin{bmatrix} \frac{1}{i\sqrt{\tilde{\mu}_k(h)}}\vec{\phi}_k(h) \\ \vec{\phi}_k(h) \end{bmatrix}\right) \tag{26}$$

where $\tilde{\mu}_k(h)$ *are the eigenvalues of* $(\boldsymbol{M}^{-1}+\boldsymbol{J}_h)\boldsymbol{A}_h^2$:

$$\tilde{\mu}_k(h)=\left(\frac{1}{\tilde{\lambda}_k(h)}+\omega_k(h)\right)\lambda_k^2(h),\ \ k=1,2,...,N,$$

with $\sqrt{\tilde{\mu}_k(h)}:=-\sqrt{\tilde{\mu}_{-k}(h)}$ *and* $\vec{\varphi}_k:=\vec{\varphi}_{-k}$ *for* $k=-1,-2,...,-N$. *The solutions to* (25) *can be expressed as*

$$\vec{z}(t)=\sum_{k\in K}(a_k e^{i\sqrt{\tilde{\mu}_k(h)}t})\vec{\phi}_k(h). \tag{27}$$

Proof. Recall that the eigenvalues of $\boldsymbol{J}_h$, and $\boldsymbol{A}_h$ are $\omega_k(h)$, and $\lambda_k(h)$ respectively, for all $k\in K$. Moreover, by Lemma 7, $\boldsymbol{M}$, $\boldsymbol{J}_h$, and $\boldsymbol{A}_h$ are simultaneously diagonalizable. Hence the eigen-pairs of $(\boldsymbol{M}^{-1}+\boldsymbol{J}_h)$ are $(\tilde{\lambda}_k+\omega_k)$. The rest of the proof follows immediately. □

The discretization of higher-order energy, (5), corresponding to (25) is as follows

$$E_{h,1}(t):=\tfrac{h}{2}\sum_{j=1}^{N}\left(\tfrac{(\boldsymbol{M}\boldsymbol{J}_h\boldsymbol{A}_h^2\vec{z})_{j+1}-(\boldsymbol{M}\boldsymbol{J}_h\boldsymbol{A}_h^2\vec{z})_j}{h}\right)\left(\tfrac{\vec{z}_{j+1}-\vec{z}_j}{h}\right)+\left|\tfrac{(\boldsymbol{M}^{1/2}\dot{\vec{z}})_{j+1}-(\boldsymbol{M}^{1/2}\dot{\vec{z}})_j}{h}\right|^2+\left|\tfrac{(\boldsymbol{A}_h z)_{j+1}-(\boldsymbol{A}_h z)_j}{h}\right|^2$$

where $\boldsymbol{M}^{1/2}$ is uniquely defined since $\boldsymbol{M}$ is positive definite.

Lemma 8. *The energy* $E_{h,1}(t)$ *is conserved along the trajectories, i.e.* $\frac{dE_{h,1}(t)}{dt}=0$. *and thus,* $E_{h,1}(t)\equiv E_{h,1}(0),\forall t\geq 0$. *Moreover,* $E_{h,1}(t)$ *can be written in terms of eigen-pairs as the following*

$$E_{h,1}(t)=h\sum_{\substack{j=0\\k\in K}}^{N}|\tilde{\lambda_k}(h)||\tilde{\mu}_k(h)||a_k|^2\left|\frac{\phi_{k,j+1}-\phi_{k,j}}{h}\right|^2. \tag{28}$$

Proof. Considering the eigenvalues of $\boldsymbol{J}_h$, $\boldsymbol{A}_h$, and $\boldsymbol{M}$ with the solution formula (27) yields the following

$$(\boldsymbol{M}^{1/2}\vec{z})_j=\sum_{k\in K}\sqrt{\tilde{\lambda}_k(h)}(a_k e^{i\sqrt{\tilde{\mu}_k(h)}t})\phi_{k,j}(h),$$
$$(\boldsymbol{M}\boldsymbol{J}_h\boldsymbol{A}_h^2\vec{z})_j=\sum_{k\in K}\tilde{\lambda}_k(h)\lambda_k^2(h)\omega_k(h)a_k e^{i\sqrt{\tilde{\mu}_k(h)}t}\phi_{k,j}(h).$$

By utilizing $\ddot{\vec{z}}=-(\boldsymbol{M}^{-1}+\boldsymbol{J}_h)\boldsymbol{A}_h^2\vec{z}$ and a straightforward calculation,

$$\frac{dE_{h,1}(t)}{dt}=h\sum_{\substack{j=0\\k\in K}}^{N}\tilde{\lambda}_k(h)i\sqrt{\tilde{\mu}_k^3(h)}a_k\left(\tfrac{\phi_{k,j+1}-\phi_{k,j}}{h}\right)$$
$$+h\sum_{j=1}^{N}\left(\tfrac{(\boldsymbol{M}^{1/2}(\boldsymbol{M}^{-1}+\boldsymbol{J}_h)\boldsymbol{A}_h^2\vec{z})_j-(\boldsymbol{M}^{1/2}(\boldsymbol{M}^{-1}+\boldsymbol{J}_h)\boldsymbol{A}_h^2\vec{z})_{j+1}}{h}\right)\times\left(\tfrac{(\boldsymbol{M}^{1/2}\dot{\vec{z}})_{j+1}-(\boldsymbol{M}^{1/2}\dot{\vec{z}})_j}{h}\right)=0,$$

which implies that $E_{h,1}(t)\equiv E_{h,1}(0),\forall t\geq 0$. Finally, (28) follows from considering $E_{h,1}(0)$ with the eigenvalues given by direct calculation. □

The corresponding discretization of the sensor measurements $\int_0^T|\dot{z}'(L,t)|^2dt$ can be expressed as follows

$$\int_0^T\left|\tfrac{\dot{z}_N}{h}\right|^2dt=T\sum_{k\in K}|\tilde{\mu}_k||a_k|^2\left|\tfrac{\phi_{k,N}}{h}\right|^2. \tag{29}$$

Theorem 9. *For any* $T>0$, *the system* (25) *is observable uniformly as* $h\to 0$. *In particular,*

$$E_{h,1}(0)=\frac{L}{2T}\int_0^T\left|\frac{\dot{z}_N}{h}\right|^2dt. \tag{30}$$

Proof. Consider Lemma 8, Eq. (16), and (29)

$$E_{h,1}(0)=h\sum_{\substack{j=0\\k\in K}}^{N}|\tilde{\lambda_k}(h)||\tilde{\mu}_k(h)||a_k|^2\left|\tfrac{\phi_{k,j+1}-\phi_{k,j}}{h}\right|^2$$
$$=\sum_{k\in K}\tfrac{2L}{4-\lambda_k(h)h^2}|\tilde{\lambda_k}(h)||\tilde{\mu}_k||a_k|^2\left|\tfrac{\phi_{k,N}}{h}\right|^2$$
$$=\tfrac{L}{2}\sum_{k\in K}|\tilde{\mu}_k||a_k|^2\left|\tfrac{\phi_{k,N}}{h}\right|^2=\tfrac{L}{2T}\int_0^T\left|\tfrac{\dot{z}_N}{h}\right|^2dt.\quad\square$$

Remark 3. Notice that the lower-order energy of the model obtained by the Order-Reduced Finite Differences (25) is

$$E_{h,-1}(t):=\tfrac{h}{2}\sum_{j=1}^{N}\left|\tfrac{(\boldsymbol{M}^{1/2}\boldsymbol{A}_h^{-1}\dot{\vec{z}})_{j+1}-(\boldsymbol{M}^{1/2}\boldsymbol{A}_h^{-1}\dot{\vec{z}})_j}{h}\right|^2+\left|\tfrac{z_{j+1}-z_j}{h}\right|^2+\left(\tfrac{(\boldsymbol{M}\boldsymbol{J}_h\boldsymbol{A}_h\vec{z})_{j+1}-(\boldsymbol{M}\boldsymbol{J}_h\boldsymbol{A}_h\vec{z})_j}{h}\right)\times\left(\tfrac{(\boldsymbol{A}_h^{-1}\vec{z})_{j+1}-(\boldsymbol{A}_h^{-1}\vec{z})_j}{h}\right).$$

Therefore, following Remark 1, the standard sensor measurement $\int_0^T\left|\frac{z_N}{h}\right|^2dt$ with $E_{h,-1}(t)$, as in [11], proceeds to the lack of uniform observability as $h\to 0$. Therefore, the time derivative in the sensor measurement is essential for the Order-Reduction method in proving the observability result.

IV. Simulations & Numerical Experiments

To show the strength of the proposed model reductions (10),(18) and (25), consider the observed boundary measurement (15) fed back to the moment boundary condition, i.e. $z_{N+2}+z_N=\xi\dot{z}_N$, with a positive feedback gain, $\xi>0$. For the PDE counterpart (1), it simply is $z''(L,t)=-\xi\dot{z}'(L,t)$. The closed-loop system can be shown to be exponentially stable. The layers of the multi-layer beam are numbered from one to five, with the choice of materials being, respectively, PZT, silicon rubber, aluminum alloy, epoxy, copper. $\boldsymbol{B}$, $\boldsymbol{C}$ and $\boldsymbol{P}$ matrices corresponding to the material constants in Table IV are calculated, i.e. $\boldsymbol{B}\approx\begin{bmatrix}32\\168\end{bmatrix}$, $\boldsymbol{C}\approx\begin{bmatrix}16&0\\0&92\end{bmatrix}$, $\boldsymbol{P}\approx\begin{bmatrix}249&-368\\-368&2391\end{bmatrix}$.

		Layers				
Material Constant	Unit	1	2	3	4	5
Mass density	$\frac{kg}{m^3}(\times 10^3)$	7.5	1.24	2.81	1.19	8.66
Thickness	$m(\times 10^{-2})$	2	3	4	4.5	3.5
Young's Modulus	GPa	89	0.08	71.1	35.2	117
Shear Modulus	GPa	27	0.511	26.8	1.96	44.2
Poisson's Ratio		0.31	0.5	0.33	0.38	0.32

The simulations are considered for $N=30$ nodes ($h=\frac{1}{31}\approx 0.032$), $T=0.1$ sec, and $L=1$m. The initial conditions are $z_0(x_i)=z_1(x_i)=10^{-3}\sum_{j=15}^{30}jh\sin(jh\pi x_i)$.

In the plots below, the model reductions are shown with their abbreviations, i.e. Standard Finite Differences (SFD) and Order-Reduced Finite Differences (ORFD).

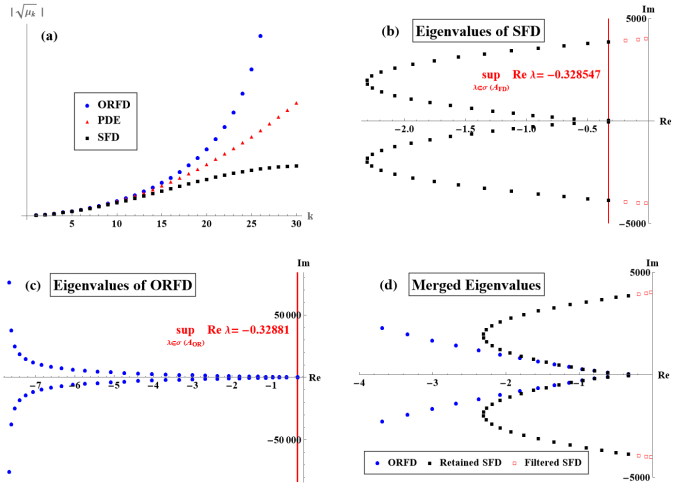

Fig. 1. (a) For $\xi \equiv 0$, modulus of conservative eigenvalues of PDE, SFD, ORFD. For $\xi = 0.002$, (b) eigenvalues of SFD with/without filtering, (c) ORFD, and (d) all overlapping into one plot.

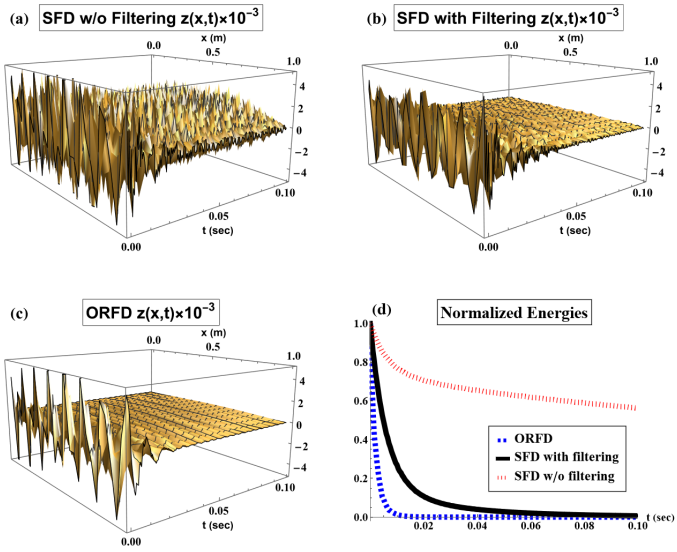

Fig. 2. For $\xi = 0.002$, the solution $z(x,t)$ of (a) SFD without filtering ($\gamma = 4$), (b) SFD with filtering ($\gamma = 3.8$), and (c) ORFD. (d) The normalized energies are plotted for each case. Refer to [2] for real-time simulations of various initial data and material parameters.

In the case of no boundary damping, i.e. $\xi \equiv 0$, the PDE model (1) has only purely imaginary eigenvalues $\{\mp i\sqrt{\mu_k}\}_{k=1}^{\infty}$ with a uniform gap among the consecutive eigenvalues. The moduli of the eigenvalues for each model reduction are plotted in Fig. 1_a. Since the high-frequency SFD eigenvalues flatten, it causes the lack of uniform gap as $h \to 0$. This is not observed for the ORFD model at all, i.e. the gap does not converge to zero as $h \to 0$.

As seen in Figs. $2_{b,c,d}$, in the case of boundary damping, i.e. $\xi = 0.002$, the high-frequency vibrational modes of $z(x,t)$ and the overall energy of the unfiltered ($\gamma = 4$) SFD model are resistant to the boundary controller since the high-frequency eigenvalues approach the imaginary axis, i.e. $\max \mathrm{Re}\mu_k^{SFD} \approx -0.02$, see Fig. 1_b. After even slight filtering ($\gamma = 3.8$), six highest-frequency eigenvalues are filtered out. Thus, the solution $z(x,t)$ and the overall energy exponentially decay to zero. Indeed, the filtering ensures that eigenvalues get bounded away from the imaginary axis, i.e. $\max \mathrm{Re}\mu_k^{SFD} \approx -0.3285$.

As seen in Figs. $2_{c,d}$, the solution $z(x,t)$ and the overall energy of the ORFD decay exponentially to zero, without any additional filtering. The reason can be seen in spectral plot in Fig. 1_c. All eigenvalues are already uniformly bounded away from the imaginary axis, i.e. $\max \mathrm{Re}\mu_k^{ORFD} \approx -0.3288$.

V. Ongoing & Future Work

The exponential stability of the model (1) with cantilevered boundary conditions is recently investigated [9] by Finite Differences. The spectral methods are all inapplicable since finding the spectrum of the system operator explicitly (in terms of h) is not possible. The Order-Reduction algorithm with this set of boundary conditions works pretty good as in [6], [7]. The exact controllability and exponential stabilizability problems are currently under investigation.

The rigorous proof of the exponential stability of the closed-loop model considered in Section IV is currently under investigation as well. The proof requires non-trivial and successive uses of discrete multipliers.

References

[1] A.A. Allen, S.W. Hansen, *Analyticity and optimal damping for a multilayer Mead-Markus sandwich beam,* Discrete Contin. Dyn. Syst.- B, (14-4) 2010, 1279-1292.

[2] A.K. Aydin, M. Poynter, A. Ö. Özer Vibration Suppression on a Hinged Three-Layer Sandwich Beam, Wolfram Demonstrations Project, Published: January 2, 2023.

[3] S.W. Hansen, R. Fabiano, *Modeling and analysis of damped three-layer beams*, Discrete and Continuous Dynamical Systems, 2001, 143-155.

[4] J.A Infante, E. Zuazua, Boundary observability for the space semi-discretizations of the 1-D wave equation, *Math. Model. Num. Ann.*, (33) 1999, 407-438.

[5] L. Leon, E. Zuazua, *Boundary controllability of the finite-difference space semi-discretizations of the beam equation,* ESAIM Control Opt. Calc. Var., (8) 2002, 827-862.

[6] J. Liu, B.Z. Guo, A novel semi-discrete scheme preserving uniformly exponential stability for an Euler Bernoulli beam, Systems & Control Letters, (134) 2019, 104518.

[7] J. Liu, B.Z. Guo, *Uniformly semi-discretized approximation for exact observability and controllability of one-dimensional Euler-Bernoulli beam,* Systems & Control Letters (156) 2021, 105013.

[8] J. Liu, B.Z.Guo, *A new semi-discretized order reduction finite difference scheme for uniform approximation of 1-d wave equation,* SIAM Journal on Control and Optimization, (58) 2020, 2256-228.

[9] A.Ö. Özer, *Exponential stabilization of a smart piezoelectric composite beam with only one boundary controller,* 6^{th} IFAC Proceedings, Valparaiso, Chile, (51-3) 2018, 80-85.

[10] A.Ö. Özer, *Uniform boundary observability of semi-discrete finite difference approximations of a Rayleigh beam equation with only one boundary observation,* 58th IEEE Conference on Decision and Control (CDC), 2019, 7708–7713.

[11] A.Ö. Özer, A.K. Aydin, Uniform boundary observability of filtered finite difference approximations of a Mead-Marcus sandwich beam equation with only one boundary observation, 61^{st} IEEE Conference on Decision and Control, Cancun, Mexico, 2022, 6535-6541.

[12] A.Ö. Özer, S.W. Hansen, Exact boundary controllability of an abstract Mead-Marcus sandwich beam model, 49^{th} IEEE Conference on Decision and Control, Atlanta, GA, 2010, 2578–2583.

[13] R. Rajaram, Moment method in distributed control theory, M.Sc. Thesis, Iowa State University, 2003.

[14] H.J.Ren, B.Z.Guo, *Uniformly exponential stability of semi-discrete scheme for observer- based control of 1-D wave equation,* Systems & Control Letters, 168 (2022), 105346.

[15] E. Zuazua, *Propagation, observation, control and numerical approximation of waves approximated by finite difference method,* SIAM Review (47) 2005, 197243.